EurJOC
European Journal of Organic Chemistry

Research Article
doi.org/10.1002/ejoc.202300863

Chemistry Europe
European Chemical Societies Publishing

www.eurjoc.org

Hybrid Steroid-[60]Fullerene as n-Type Material for Organic Photovoltaics

Reinier Lemos,[a] Yoana Perez-Badell,[b] Orlando Ortiz,[a] Luis Almagro,[a] Hortensia Rodríguez,[c] María Ángeles Herranz,[d] Margarita Suarez,*[a] and Nazario Martín*[d, e]

Fullerene derivatives have been used as electron acceptor and transport materials in organic photovoltaics as well as in perovskite solar cells. Among them, [6,6]-phenyl-C_{61}-butyric acid methyl ester ($PC_{61}BM$) has been one of the most widely used, in combination with poly-3-hexylthiophene (P3HT) as an electron donor semiconducting polymer, for the fabrication of organic bulk heterojunction solar cells (BHJ-OSC). In this work, a steroid-fullerene hybrid was synthesized through the Bingel–Hirsch reaction to compare its properties with $PC_{61}BM$ as the reference structure. Different spectroscopic techniques were employed to characterize the new fullerene derivative, namely 1D and 2D nuclear magnetic resonance (NMR), Fourier Transform Infrared Spectroscopy (FTIR), and high-resolution mass spectrometry (HRMS). In addition, thermogravimetric analysis (TGA), and cyclic voltammetry were also performed. The characterization was completed by transmission electron microscopy (TEM), which explore the hybrid's morphology, where the presence of the steroid moiety increases the solubility of the fullerene material. DFT/PBE–D3(BJ)/6-311G(d,p) calculations for both the steroid-fullerene hybrid and $PC_{61}BM$ allowed to obtain geometry optimizations and electronic structure data. A comparative study to analyze the nature of the electronic properties of the synthesized steroid-[60]fullerene hybrid and $PC_{61}BM$ with an oligomer of ten thiophene units, used in the active layer of organic solar cells, was carried out. Electron density maps using the [CIS|CNDOL/21] approach illustrate the photoexcitation of the donor followed by an electron-charge transfer to the acceptor fullerene.

Introduction

Over the past few decades, the increasing world energy demand, combined with the fast depletion of fossil fuels,[1,2] has led to the scientific community to seek for renewable and clean energy sources. In this regard, solar energy has been considered one of the most promising alternatives in the foreseeable future.[3,4,5] Thus, it is estimated that by the year 2050 the 20% of the global energetic demand will be supplied by photovoltaic technology.[6]

Organic-based optoelectronic devices, have attracted considerable interest as an alternative to complement silicon or perovskite-based devices, due to their easy solution processing methods on flexible substrates.[7] Besides their lightweight, flexibility and semi-transparent properties, the production scalability in large-area devices, such as photovoltaic panels, is an interesting advantage of organic photovoltaics.[8–11] In addition to these benefits, their energy payback times are substantially shorter than those achieved in single-crystal silicon solar cells.[12]

The combination of donor and acceptor molecular systems is of interest for a wide variety of organic photovoltaic devices or in the construction of artificial photosynthetic architectures.[13] As yet, bulk-heterojunction (BHJ) structures, with combined solid blends of two types of semiconductors, an electron donor (*p*-type), and an electron acceptor (*n*-type), have dominated the Organic Solar Cells (OSC).[14] In this kind of architectures, the mixture of the donor and acceptor materials shows the tendency to form bicontinous interpenetrating networks from spontaneous nanoscale phase separation. This factor is a crucial step to get a high carrier mobility and,

[a] *Dr. R. Lemos, O. Ortiz, Dr. L. Almagro, Prof. Dr. M. Suarez*
Laboratorio de Síntesis Orgánica
Facultad de Química
Universidad de la Habana
10400 La Habana (Cuba)
E-mail: msuarez@fq.uh.cu
Homepage: http://www.fq.uh.cu

[b] *Dr. Y. Perez-Badell*
Laboratorio de Química
Computacional y Teórica
Facultad de Química
Universidad de La Habana
10400 La Habana (Cuba)

[c] *Dr. H. Rodríguez*
Yachay Tech University
School of Chemical Sciences and Engineering
100119 Urququi (Ecuador)

[d] *Dr. M. Á. Herranz, Prof. Dr. N. Martín*
Departamento de Química Orgánica
Facultad de Ciencias Químicas
Universidad Complutense de Madrid
28040 Madrid (Spain)
E-mail: nazmar@ucm.es
Homepage: http://nazariomartingroup.com

[e] *Prof. Dr. N. Martín*
IMDEA-Nanociencia
Campus de Cantoblanco
28049 Madrid (Spain)

Supporting information for this article is available on the WWW under https://doi.org/10.1002/ejoc.202300863

Research Article
doi.org/10.1002/ejoc.202300863

therefore, to achieve better values of power conversion efficiency (PCE).[15]

Donor–acceptor organic bulk heterojunctions are promising systems for developing photovoltaic devices. Organic solar cells utilize a donor-acceptor system to break up excitons into free carriers. In the bulk heterojunction (BHJ) structure, these donor-acceptor materials are intimately mixed to ensure that all generated excitons reach an interface before recombining.[16,17,18]

In recent years, there have been impressive advances in improving the structure of OSC to increase performance, resulting in a power conversion efficiency (PCE) up to 18% in OSC and up to 25% in the OSC combined modules.[19,20]

Fullerene derivatives have been used as acceptor materials in solar cells for over two decades, following the demonstration of the first proof of-concept devices at the end of the last century.[21]

The electronic features of C_{60} and C_{70} molecules are remarkable: a lowest unoccupied molecular orbital (LUMO) delocalized over the whole surface, and the ability to accept and transport electrons in three dimensions, which facilitates electron delocalization at the donor-acceptor interfaces in BHJ solar cells.[22] Employing fullerene derivatives as *n*-type semiconductor enables an increase in the open circuit voltage (V_{oc}) of the corresponding photovoltaic cells, at the time that PCE values of around a 14% could be easily achieved.[23]

One remarkable example of a soluble fullerene derivative is the 1-(3-methoxycarbonyl)propyl-1-phenyl[6,6]C_{61} ($PC_{61}BM$), synthesized by Wudl et al. (Figure 1),[24] which is the most widely used fullerene derivative as electron acceptor in solar cells, field-effect transistors and photodetectors.[25]

Important criteria in the design of new fullerene derivatives as improved *n*-type transport layers have been the search for a reduced electron affinity and the solubility increase in organic solvents.[26] In this sense, several fullerene derivatives have been reported, such as [6,6]-phenyl-C_{61} butyric acid 2-ethylhexyl ester ($PC_{61}BEH$) where was demonstrated that the branched alkyl chain of the fullerene derivative can highly influence the solubility (Figure 1).[27]

Currently, a renaissance of fullerene-based materials is observed with their use in multicomponent organic solar cells and perovskite solar cells, where they play an important role as electron transport materials. The success in both of these devices requires the tunability of the optoelectronic characteristics of fullerene derivatives.[28] Their use as electron extraction and transport materials, as well as their solution processing in OSCs devices has been clearly demonstrated in recent reports.[29]

However, in general, fullerene derivatives are not soluble in water and have a low solubility in most organic solvents. The attachment of organic addends with polar groups in their structure, such as steroids, might be a common strategy in the pursuit of fullerene conjugates with a better solubility.[30,31]

So far, and to the best of our knowledge, despite the interesting properties as a molecular scaffold of steroids, there is only one steroid-fullerene material analogue to $PC_{61}BM$, the 1-(3-carboxypropyl)-l-phenyl[6.6]C_{61}cholestanyl ester ($PC_{61}BM$-Col), reported (Figure 1).[24] This is one of the most soluble methanofullerenes prepared at the time.

In the design of organic bulk heterojunctions, it is also very important the donor material of choice. Large molecular donors, such as thiophene oligomers, have been widely used in solar cells.[32] Also, donor-acceptor heterojunctions composed of thiophene oligomers and [60]fullerene were investigated with computational methods.[33]

The production of bulk heterojunction solar cells (BHJ-OSC) from poly(3-hexylthiophene) (P3HT) and [6,6]-phenylC_{61} butyric acid methyl ester ($PC_{61}BM$) with power efficiencies of over a 4% has been reported.[34] Electronic structure calculations were used to provide strategies for designing P3HT-fullerene derivative-based donor-acceptor materials for use in high-efficient BHJ-OSC.[35]

Considering our interests in the chemistry of fullerene and our expertise in steroids, herein, we report a straightforward synthetic methodology to obtain a novel hybrid material from the reaction of suitably functionalized epiandrosterone with [60]fullerene. Epiandrosterone is an important naturally occurring steroid hormone suited with and hydroxyl group able to easily be transformed in a malonic ester. This ester is the precursor of a steroid-[60]fullerene cyclopropane monoadduct that bears similar linkers that $PC_{61}BM$-Col, with additional ester and carbonyl functional groups in the structure.

According to the results obtained from cyclic voltammetry (CV), transmission electron microscopy (TEM), thermogravimetric analysis (TGA), and theoretical studies, the steroid-[60]fullerene material synthesized could be employed as a n-type semiconductor in OSC. Using the approximated CNDOL method together with configuration interaction of single excitations [CIS|CNDOL/21],[36] a comparative study was carried out to analyze the nature of the electronic properties of the synthesized hybrid and $PC_{61}BM$ with an oligomer of ten thiophene units, used in the active layer of OSC.[37]

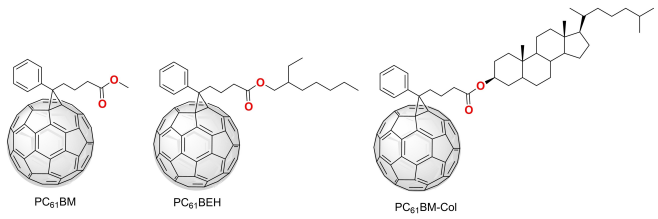

Figure 1. Molecular structures of PCBM-based derivatives.

Results and Discussion

The synthesis of the new steroid-methano[60]fullerene **5** (Scheme 1) was carried out through a multistep synthetic route in which the pristine C_{60} was covalently linked to the steroid moiety by a cyclopropanation reaction based on the Bingel-Hirsch protocol.

This synthetic procedure previously required the structural modification of the C3 position on the ring A of the steroid

Research Article
doi.org/10.1002/ejoc.202300863

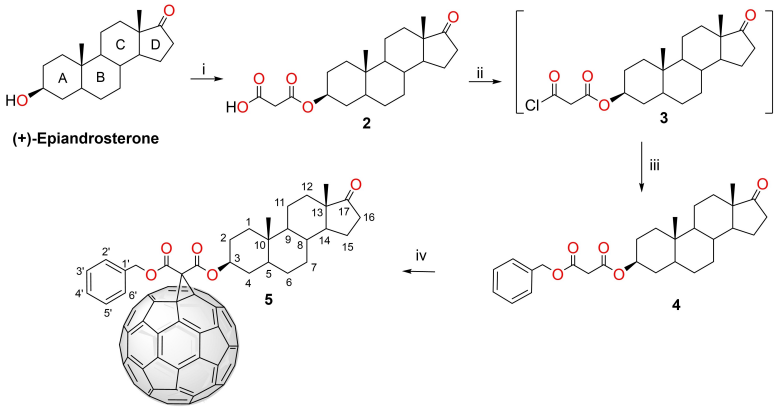

Scheme 1. Reagents and conditions: (i) Meldrum's acid, toluene, reflux, 6 h. (ii) $SOCl_2$, $CHCl_3$, reflux, 8 h. (iii) benzyl alcohol, DMAP, DCM, r.t. 24 h. (iv) C_{60}, DBU, CBr_4, toluene, r.t. 2 h.

fragment, to obtain the corresponding malonyl-steroid substituted compounds. Therefore, the first steps involve the obtention of steroid derivatives **2**–**4**, as depicted in Scheme 1. New hybrids compounds were prepared using the Bingel–Hirsch protocol in a multistep synthetic procedure (see Scheme 1).

The starting steroid for the synthetic procedure was the commercially available epiandrosterone (**1**). The synthesis of the steroid-malonate derivative **2** was carried out through a nucleophilic acyl substitution reaction between the hydroxyl group on C3 of the epiandrosterone (**1**) and Meldrum's acid, at reflux of toluene, providing the 3-oxy-(3β-5α-androstan-17-one)-3-oxopropanoic acid (**2**) with a 50% yield after purification. Afterward, the esterification of compound **2** was achieved in two subsequent steps (Scheme 1). Firstly, to get a more reactive derivate, an acyl chloride (**3**) was formed from **2**, employing thionyl chloride as acylating agent and carrying out the reaction in refluxing chloroform. Due to the low stability of compound **3**, it was not isolated and was subsequently used in the reaction with benzyl alcohol. This transformation employed N,N-dimethylaminopyridine (DMAP) as catalytic base, and dichloromethane (DCM) as solvent, and the 3β-benzylmalonate-5α-androstan-17-one (**4**) was obtained with a 42% yield after purification by column chromatography using a mixture of *n*-hexane/ethyl acetate (5:1) as eluent.

The newly synthesized compounds were fully characterized, by different analytical and spectroscopic techniques (see Experimental Section and Supporting Information). ^{1}H NMR spectroscopy reveals the signal corresponding to the proton H3 of the steroid moiety (ring A) in compound **2**, as a multiplet at $\delta = 4.81$ ppm, while this proton in the starting steroid **1** appears at 3.55 ppm. In both cases, the methylene protons of the malonate fragment appear as singlets at $\delta \approx 3.4$ and 3.3 ppm for compounds **2** and **4**, respectively. Furthermore, the signals corresponding to the aromatic protons in derivate **4** were observed over 7.00 ppm (see Experimental Section and Supporting Information).

The ^{13}C NMR spectra of **2** and **4** show the presence of the two carbonyl groups at $\delta \approx 169$ and 165 ppm, whereas the signals assigned to the methylene carbon appear at $\delta \approx 40$ and 41 ppm, respectively. Besides, for the malonate-steroid derivate **4** four signals in the sp^2 carbon region were assigned to the aromatic carbons. Moreover, at $\delta = 67.11$ ppm appears the signal corresponding to the carbon of the benzylic position (see Experimental Section).

Mass spectrometry further confirmed the chemical structures of the new compounds. Under electrospray ionization (ESI) conditions, $[M+Na]^+$ peaks at m/z = 399.1 and 489.2, where obtained for compounds **2** and **4**, respectively.

The covalent attachment of the malonate **4** to [60]fullerene was carried out by a cyclopropanation reaction under Bingel-Hirsch conditions in the presence of CBr_4 and 1,8-diazabicyclo[5.4.0]undec-7-ene (DBU) at room temperature (Scheme 1). After the DBU was added, the color solution of the reaction shifted from purple to brown, which evidences the formation of the mono-adduct [6,6]-closed, as expected.[38,39]

The reaction progressed rapidly, and after 2 h the obtention of the new fullerene derivative was completed. After purification by flash chromatography, at first with carbon disulfide to elute the unreacted C_{60}, followed by DCM, compound **5** was obtained, as a stable brown solid, with 66% yield. Interestingly, the conjugation of the epiandrosterone moiety to C_{60} improves the solubility of C_{60} in organic solvents such as chloroform, dichloromethane, and dimethylformamide, among others.

The HPLC chromatogram of the reaction mixture (toluene/acetonitrile 9:1; 1 mL min^{-1}, Figure S25 in Supporting Information) shows two major peaks at ca. 4.0 and 8.7 min, corresponding to compound **5** and to the C_{60} starting material, respectively. This assignment was possible through the different UV-Vis spectra that both molecules have. In the case of the mono-adduct, the spectrum presents a weak absorption band at approximately 430 nm characteristic of [6,6]-mono-adducts.[40] (see Figure S26 in the Supporting Information).

The chemical structure of the new steroid-fullerene material **5** was determined unambiguously by ^{1}H NMR, ^{13}C NMR, COSY, DEPT, HSQC, and HMBC (see Experimental Section and Supporting Information).

Research Article
doi.org/10.1002/ejoc.202300863

Chemistry Europe
European Chemical Societies Publishing

The ^{1}H NMR spectrum revealed the disappearance of the methylene protons in the hybrid **5**, which appear at 3.39 ppm for compound **4**. In addition to the expected signals corresponding to the steroid moiety, a deshielding in the signals of the aromatic protons and the proton on C3 of the ring A of the steroid fragment were observed (see Experimental Section). This behavior is due to the paramagnetic currents of the C_{60} backbone. Moreover, it is worth highlighting the signal at 5.51 ppm corresponding to the protons of the benzylic position. The multiplicity of this position shifted from a singlet in hybrid **4** to a doublet of doublets, with a coupling constant of 11.8 Hz, in material **5**, as a consequence of the loss of chemical equivalency and the development of an AB system in compound **5**, instead of the A2 system in malonate **4**, due to the influence of the [60]fullerene. The presence of the C_{60} moiety does not affect the other proton signals of the steroid motif (see Experimental Section).

On the other hand, ^{13}C NMR spectrum of **5** reveals an increased number of signals in the sp^2 carbon region, due to the lack of symmetry of the C_{60} backbone when it was attached to the malonate-steroid moiety **4**. Furthermore, at $\delta \approx 162$ and 163 ppm appear the signals corresponding to the carbonyl groups of the malonate moiety. Meanwhile, at 71.60 and 71.58 ppm the signals of the sp^3 carbon atoms of the cyclopropane ring are shown, whereas the signal of the quaternary carbon atom appears at 52.15 ppm. The positions of the other steroid carbon atoms are relatively insensitive to the presence of the [60]fullerene cage. The only exception is the case of C3 on the steroid A ring, which is strongly deshielded (by ca. 3 ppm) related to malonate **4**, due to the presence of the C_{60} sphere. Finally, to confirm the chemical structure of **5**, an unambiguous assignment of ^{1}H and ^{13}C NMR resonances was carried out by a combination of HMQC and DEPT data. Quaternary carbon atoms were assigned by analysis of the HMBC spectra (see Experimental Section and Supporting Information).

HRMS supported the proposed structure. The MALDI-TOF spectrum of compound **5** shows a peak at $m/z = 1184.25532$, which nicely corresponds with its molecular ion $[M-H]^-$ (see Figure S23 in Supporting Information). Finally, the FTIR spectra of compound **5** showed a C=O stretching vibration at around 1737 cm^{-1}, and the characteristic band of organofullerene derivatives at ca. 730 cm^{-1}.[41] (See Figure S24 in Supporting Information).

The study of the redox properties of the fullerene derivatives is fundamental to determine their electronic properties. The electrochemical behavior of methanofullerene **5** was studied by cyclic voltammetry (CV) using THF as solvent. The reduction potentials calculated from CV vs. Fc/Fc$^+$ are given in Table 1.

Table 1 shows the reduction potentials of C_{60}, a Bingel-Hirsch diethylmalonate-C_{60} monoadduct and $PC_{61}BM$ as references, and the hybrid **5**. Four reduction steps were observed in the voltammogram of derivative **5** (see Figure S27 in the Supporting Information). Two well-defined reversible reduction waves are obtained, while the third and fourth reduction steps are chemically irreversible, most probably due to the reductive cleavage of one of the [6,6] bonds of C_{60} and the organic addend.[44]

Table 1. Electrochemical properties of hybrid **5**, C_{60}, $PC_{61}BM$ and Bingel-Hirsch diethylmalonate-C_{60} monoadduct (DEM-C_{60}).

Compound[a]	$E^1_{1/2,\,red}$	$E^2_{1/2,\,red}$	$E^3_{1/2,\,red}$	LUMO[e]
C_{60}[b]	−0.86	−1.44	−2.00	−4.24
$PC_{61}BM$[c]	−1.00	−1.59	−2.19	−4.10
DEM-C_{60}	−0.94	−1.47	−2.03	−4.16
5	−0.92	−1.48	−2.09[d]	−4.18

[a] Potentials in V vs. Fc/Fc$^+$ measured with CV in THF as solvent. GCE as working electrode, Pt as the counter electrode, $Ag/AgNO_3$ as the reference electrode, $TBAPF_6$ (0.1 M) as supporting electrolyte, 100 mV/s scan rate. Experimental error ±0.01 V. [b] Values obtained using $TBAPF_6$ (0.2 M). [c] From reference [42]. [d] Cathodic peak potential, irreversible process. [e] Values in eV estimated using the following equation: $LUMO = -(E^1_{1/2}\ red + 5.1)$.[43]

As shown in Table 1, the reduction potentials of **5**, the Bingel- Hirsch diethylmalonate-C_{60} monoadduct (DEM-C_{60}), and $PC_{61}BM$ are cathodically shifted related to C_{60} (between 80–140 mV of $E^1_{1/2}$, red), due to the saturation of a double bond during mono-adduct formation. This process leads to an increase of the LUMO energy as well as a decrease in the electronic affinity[45] of the monoadducts compared to [60]fullerene under the same experimental conditions.[46] Moreover, Bingel-Hirsch adducts exhibit a slightly better electron-acceptor ability than $PC_{61}BM$, with a difference among them of ca. 60–80 mV of $E^1_{1/2,\,red}$ which can be accounted for due to the presence of the two carbonyl groups connected to the cyclopropane ring. This trend is reflected in the estimated LUMO energy levels, for **5** was −4.18 eV and −4.10 eV[47] for $PC_{61}BM$ (see Table 1). If we compared the LUMO values previously calculated with the HOMO energetic level of the most commonly used donor material, P3HT (−5.20 eV),[48] the difference is 1.02 eV for hybrid **5** and 1.10 eV for $PC_{61}BM$, compound **5** could be an appropriate acceptor material for OCSs devices considering this HOMO-LUMO match.

The morphology of methanofullerene **5** was analyzed through transmission electron microscopy (TEM). To ensure a representative analysis of the sample, several areas of the grids were visualized, and representative images are presented in Figure 2.

The images obtained by TEM using the ImageJ software shown that the conjugate **5** tend to form a polydisperse system (Figure 2a), where molecular aggregates of different sizes are observed. This material's aggregation behavior is mainly associated with the hydrophobic nature of the C_{60} core as the main attractive force. This behavior is similar to those found in conjugates steroid-fulleropyrrolidine,[49] and steroids-methanofullerenes,[50] previously reported by our group.

It is noticeable that in some regions of the grids crystallization processes were observed (Figure 2b), analogous to those described for $PC_{61}BM$. The crystallinity of the nanomaterials could improve the electronic properties of nanomaterials and the performance of devices, for example, $PC_{61}BM$

Research Article
doi.org/10.1002/ejoc.202300863

Chemistry Europe
European Chemical Societies Publishing

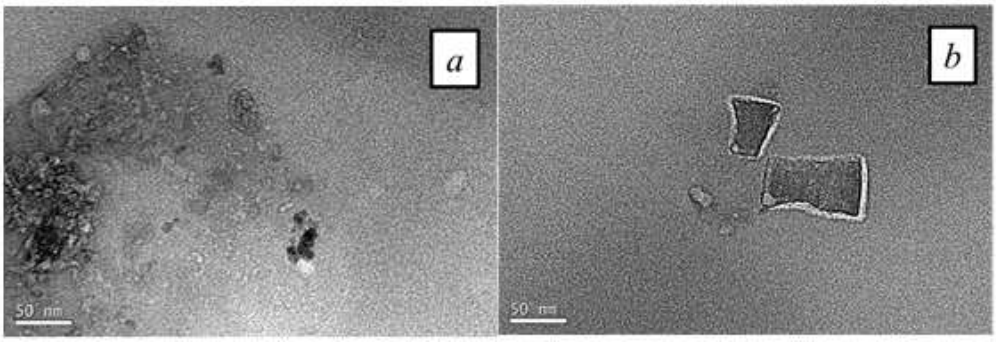

Figure 2. Representative uranyl acetate negative stain transmission electron micrographs (TEM) of compound **5**.

crystallization has shown to result in an increase in its electron affinity.[51]

The thermal stability of methanofullerene **5** was evaluated by thermogravimetric analysis (Figure S28, Supporting Information), where it is appreciated that it undergoes two initial weight losses associated to the breakdown of the steroid moiety. The first one around 300 °C and the second one at ca. 360 °C. Finally, the conjugate **5** losses at 600 °C a 90% of its total mass. Thus, if we consider that solar panels often reach temperatures over 65–85 °C,[52] this material presents the thermal stability required for organic photovoltaic devices.

For a better understanding of the geometrical and electronic properties of hybrid **5**, DFT calculations using the PBE (Perdew, Burke, and Ernzerhof) functional[53] combined with D3(BJ) Grimme's dispersion correction,[54] and the 6-311G(d,p) Pople's basis set,[55] afforded the minimum energy conformation of the structure presented in Figure 3. The PBE functional provides good results for fullerene derivatives as previously reported.[56] The Cartesian atom coordinates (Tables S1 and S2) are given in the Supporting Information.

Calculations predict a tendency to a relative *s*-trans conformation of the carbonyl groups of the malonate unit. The O═C···C═O dihedral angle has a value of −167.63°, in agreement with those previously reported for similar compounds.[57] Interaction of H3 of the corresponding ring A of the steroid moieties with the malonate carbonyl was found. The carbonyls *s*-trans conformation in the malonate moiety allows the formation of one hydrogen bond C═O···H–C3 with the hydrogen of the closest ring. The H3 distance to the oxygen from the closest carbonyl is 2.41 Å (81.9°).

Another hydrogen bond can be observed between the carbonyls from ring D and the H12 from ring C, in a twisted boat conformation with a distance of 2.41 Å. On the other hand, the phenyl group interacts with the fullerene by π–π stacking interactions at a distance of around 3.84 Å, as reported in the literature.[58] This interaction is also the dominating supramolecular force in carbon nanostructures, which are inherently constituted by large conjugated π-systems.

From the depiction of molecular orbitals (Figure 4), it can be observed that the LUMO orbitals in compound **5** are positioned exclusively on the fullerene core and the electron density of the HOMO on the steroid moiety. The calculated LUMO and HOMO

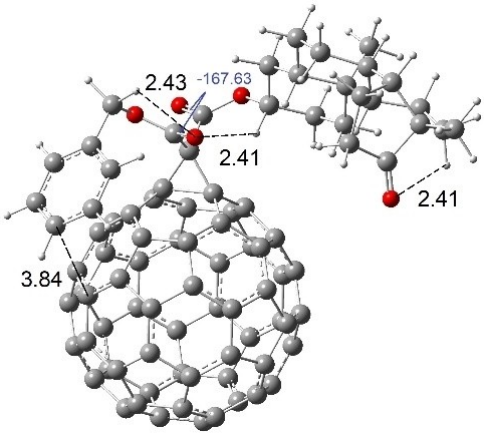

Figure 3. Minimum energy conformation of hybrid **5** obtained by the DFT-PBE method using 6–311G(d,p) basis set and D3(BJ) correction. Bond lengths are given in Å and dihedral angles in degree °.

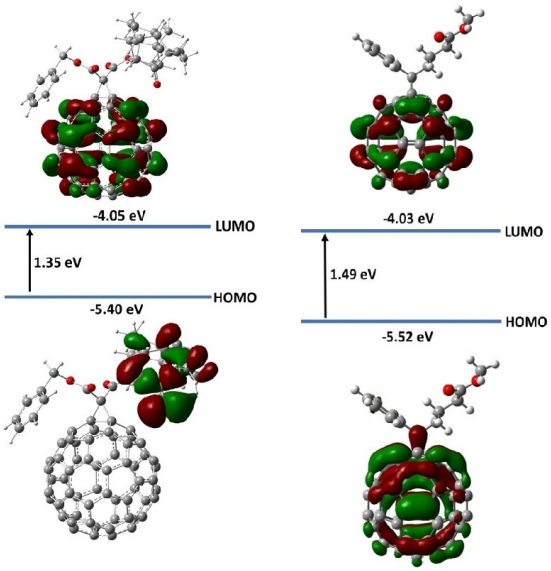

Figure 4. Molecular orbitals involved in the transitions HOMO-LUMO in compound **5** and $PC_{61}BM$, calculated using DFT method at the PBE–D3(BJ)/6-311G(d,p) level of theory in the gas phase.

Research Article
doi.org/10.1002/ejoc.202300863

energy values are −4.05 eV and −5.40 eV, respectively. A band gap of 1.35 eV has been predicted.

Comparing the experimental value from cyclic voltammetry to the LUMO estimated by DFT for **5**, we obtain close values (experimental −4.18 eV), which agrees well. As can be seen, the deviation from the experimental values is 0.13 eV.

For $PC_{61}BM$, the HOMO presents a distribution located mainly on C_{60} and almost no distribution on the chain functional group as previously reported.[59] However, the $-COOCH_3$ group induces an electron withdrawal effect as manifested by the change of HOMO electron densities in the upper part of the C_{60} core where the functional group is attached. In this case, the band gap is predicted to be 1.49 eV. Similar band gaps were found for Bingel-Hirsch steroid-free adducts (see Figure S32 in the Supporting Information for details).

The LUMO's nodal planes emerge in the middle of the fullerene core, which appears to limit the electron delocalization. The LUMO energy raised for $PC_{61}BM$ in comparison to the compound **5**. As reported,[60] this weakened electron delocalization is consistent with the contraction of system caused by C=C bond functionalization, which leads to raising LUMO levels for fullerene derivates compared with C_{60}.

Also, when the gap energy decreases, more photons at longer wavelengths can be absorbed to excite electrons to unoccupied molecular orbitals, thereby increasing the short-circuit current density. As can be deduced from Figure 4, the HOMO level of **5** is higher than the HOMO level of $PC_{61}BM$ (−5.40 vs. −5.52 eV). Furthermore, the steroid-fullerene hybrid can be considered a potential electron donor compared to $PC_{61}BM$.

The frontier molecular orbitals (HOMO and LUMO) are fundamental quantum chemical parameters, to determine the reactivity of the molecules. They are used to calculate many important properties such as chemical reactivity descriptors. Using their energy values the quantum chemical parameters such as ionization potential (I), electron affinity (A), electronegativity (χ), global hardness (η), global softness (S), electrophilicity index (ω) were calculated according to the equations reported previously.[61] Calculating the molecular descriptors for the compound **5** are useful for chemical reactivity studies, and they were performed and shown in Table 2. In this table, are also reported the values calculated for $PC_{61}BM$ at the same level of theory. For a comparison with these estimated parameters in Bingel-Hirsch steroid-free adducts see Supporting Information.

HOMO and LUMO determine qualitatively how the molecules electronically interact with other species. The obtained energy gap increases from compound **5** to $PC_{61}BM$. The last compound presents the lowest reactivity. Global softness characterizes the ability of a molecule to accept electrons. Soft molecules are of a small energy gap between frontier molecular orbitals and are more reactive than the harder ones because they can easily transfer electrons to the acceptors. Thus, the value of the global softness for hybrid **5** is 1.48 eV, while for $PC_{61}BM$ it is 1.34 eV, and the global hardness values of 0.68 eV and 0.74 eV for the **5** and $PC_{61}BM$, respectively, indicate that **5** is a better electron acceptor. Related to the electron affinity both compounds have similar ability to accept electrons, 4.05 eV (hybrid **5**) and 4.03 eV ($PC_{61}BM$). Finally, by comparing the electronegativity values, we find that compound **5** has a slightly higher value (4.77 eV) than $PC_{61}BM$ (4.72 eV), indicating that both are suitable to attract electrons from electron-donor compounds. As expected, the calculated electrophilicity values corroborate these predictions.

Table 2. Dipole moments (D) and quantum chemical parameters (eV) calculated at DFT-PBE-D3(BJ)/6-311G (d,p) level for hybrid **5** and $PC_{61}BM$.

Descriptors	Hybrid 5	$PC_{61}BM$
E_{HOMO}	−5.40	−5.52
E_{LUMO}	−4.05	−4.03
ΔE (HOMO-LUMO)	1.35	1.49
Electronegativity (χ)	4.77	4.72
Global hardness (η)	0.68	0.74
Global Softness (S)	1.48	1.34
Electrophilicity (ω)	8.48	7.55
Ionization potential (I)	5.40	5.52
Electron affinity (A)	4.05	4.03
Dipole moment [(μ)	5.91	4.19

The higher value of the calculated dipole moment of compound **5** (5.91 D) compared to $PC_{61}BM$ (4.19 D) is expected to enhance the interface contact between the material and the polymer in the device. The molecular electrostatic potential (MEP) map depicted in Figure 5 indicates that the malonate-steroid core, covalently connected to the C_{60} cage modifies the electrostatic potential distribution. Different colors at the MEP surface represent the different values of electrostatic potential. In this context, the red zone correlated with the oxygen atoms in the two carbonyl groups, indicating a negative density site in compound **5**. In contrast, the presence of the carbonylmethoxy group in the $PC_{61}BM$ side chain, decreases the polarization in the molecule, making the dipole moment's value smaller.

The theoretical and electrochemical results, the formation of crystalline domains, and the thermal stability that **5** presents in the range of 65–85 °C, allow inferring that it could have a potential use in organic photovoltaic devices. In addition to these experimental results, it was decided to analyze the nature

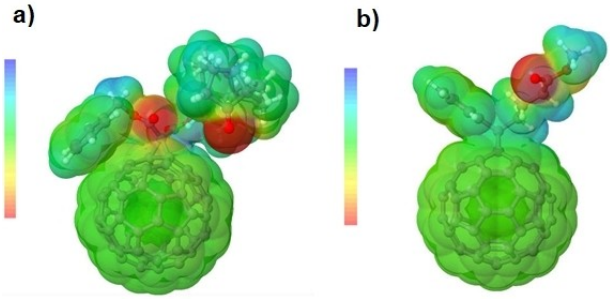

Figure 5. MEP maps of compound **5** (a) and $PC_{61}BM$ (b) obtained by CNDOL using optimized structure at DFT level. The red color represents negative potential, the blue color the positive potential and the green color the uncharged regions.

Research Article
doi.org/10.1002/ejoc.202300863

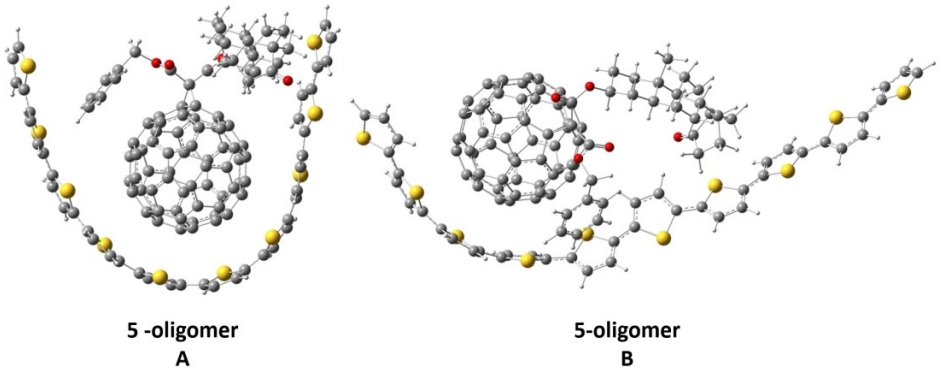

Figure 6. Optimized minimum energy structures of two **5**-oligomer complexes (A and B) by the DFT/PBE/6-311G(d,p) method.

of the interactions of **5** and $PC_{61}BM$ with an oligomer of ten thiophene units, which is a special class of donor with a high optical density as polymeric material, and similar to those employed in some of the most efficient organic heterojunctions.[62] In addition, the presence of the steroid moiety might improve C_{60} solubility and processability, ensuring a better morphology of the blend film, which constitutes an important factor in solar cells fabrication. The Cartesian atom coordinates (Tables S3 and S4) are given in the Supporting Information.

The optimized structures with two different orientations of the **5**-oligomer complex are depicted in Figure 6 and were optimized at the DFT level using the PBE functional, D3(BJ) dispersion correction and the 6-311G(d,p) base. The geometry of the 10-thiophene oligomer showed an alternation in the position of the thiophene monomers, which is not affected by the presence of **5**. The average twisted angle (S–C–C–S) between thiophene monomers remains around the 155° reported previously.[63] Van der Waals forces, particularly π–π and H-interactions, are the main factors that govern this complex orientation. The conformation where the oligomer is extended and interacting with the steroidal skeleton (**5**-oligomer B) was slightly more stable.

The interaction energies calculated for the **5**-oligomer (−29.65 kcal/mol (−20.72 kcal/mol with BSSE correction)) and for the $PC_{61}BM$-oligomer (−26.50 kcal/mol (−19.62 kcal/mol, with BSSE correction)) suggest a higher interaction strength with the steroidal derivative.

When looking at the molecular orbitals (Figure 7), the LUMO is located exclusively in the fullerene core and the HOMO electron density in the thiophene oligomer. The energy values of the HOMO and LUMO orbitals calculated for the complex **5**-oligomer are −4.60 eV and −3.91 eV, respectively. For the $PC_{61}BM$-oligomer −4.45 eV (HOMO) and −3.88 eV (LUMO) were obtained, which provides a band gap of 0.69 eV and 0.57 eV for the complexes **5**-oligomer and $PC_{61}BM$-oligomer, respectively. The higher energy gap indicates a harder and more stable complex for the **5**-oligomer.

We applied the approximate CNDOL Fockian, together with configuration interaction of single excitations (CIS), to investigate the electronic properties of the fullerene derivate with

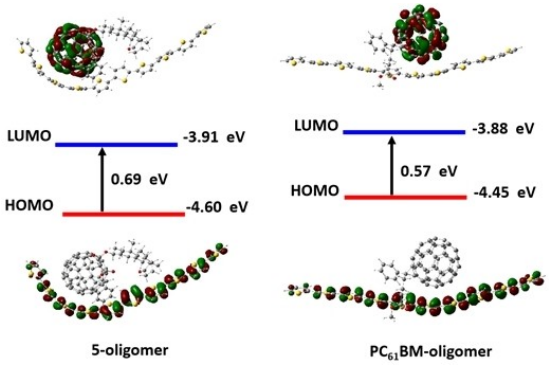

Figure 7. Molecular orbitals involved in the HOMO-LUMO transitions for the $PC_{61}BM$-oligomer and **5**-oligomer complexes obtained at the DFT/PBE–D3(BJ)/6-311G(d,p) level.

the thiophene oligomer complexed as isolated supramolecular systems, as potential candidates for photovoltaics devices. This method is validated as a valuable tool for modeling structure-related properties of molecular excitation in cases of relatively large supramolecular systems.[64]

As shown in Figure 8, the covalent attachment of the steroid moieties to the fullerene cage induced a change in the electrostatic potential distribution due to a weak charge separation. In this regard, for compound **5** in the ground state, the negative potential, represented by red color, was mainly associated with the oxygen atoms belonging to carbonyl functions. In contrast, positive regions marked by blue were located at some parts of the steroid backbone. For higher excited states, a charge transfer located mainly inside the fullerene cage was observed.

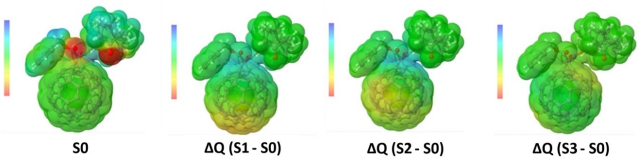

Figure 8. Depiction of the molecular electrostatic potential maps for the ground state (S0) and excited states (S1, S2 and S3) with respect to the ground state for the minimum energy structure of compound **5** at the CNDOL level.

Research Article
doi.org/10.1002/ejoc.202300863

Spectral values for compound **5** and $PC_{61}BM$ obtained by the CNDOL method are shown in Table S7. The electron charge maps of the calculated lowest energy states of compound **5** (Figure S29) and $PC_{61}BM$ Figure S30 are given in the Supporting Information.

Photoexcitation of the complex leads to an electron transfer in the system depending on the supramolecular structure. Therefore, the lower energy excited states can lead to a charge transfer (CT) from the donor to the acceptor. According to the [CIS|CNDOL/21] approach of the **5**-oligomer and $PC_{61}BM$-oligomer complexes, the energies of the first three excited states appear in Table 3 and their graphical charge displacements in Figure 9.

Electron charge maps of the lowest energy states of isolated 10-thiophene oligomers have been previously reported.[36] These results indicate that the greatest calculated electron population appears localized over the S atoms in the polymer chain at the ground state, favoring a bond-length alternation.

For the **5**-oligomer complex, the excitation to the S1 state corresponds mainly to a HOMO→LUMO electron transfer of 52%, and for the $PC_{61}BM$-oligomer of 70%. After the excitation, the first excited state shows a slight charge transfer character from the donor oligomer to **5**. For **5**-oligomer this character was observed across the first three excited states, the lowest at around 2.73 eV. In this way, the charges tend to delocalize throughout the complex, opening up the possibility of dissociation processes of an exciton, where the charge separates even in the initially excited states.

Table 3. Spectral values of the **5**-oligomer and $PC_{61}BM$/oligomer complexes obtained by the CNDOL method.

5-oligomer	E	E^{CE}	$PC_{61}BM$-oligomer	E	E^{CE}
S1	2.73^{s}	1.75	S1	2.47^{s}	1.87
S2	2.74^{w}	2.34	S2	2.71^{w}	2.35
S3	2.80^{m}	2.29	S3	2.75^{m}	2.57

E (eV) is the transition energy, E^{CE} (eV) is the corresponding calculated Coulomb–exchange term after CIS. Intensities of calculated transitions are s = strong, m = medium and w = weak.

The S1 energies for the complexes are ordered as ES1(**5**-oligomer) > ES1($PC_{61}BM$-oligomer). The lowest charge transfer state lies 0.01 eV above S1 for **5**-oligomer and 0.24 eV above S1 for $PC_{61}BM$-oligomer. For **5**-oligomer complex degeneracy originated from fullerene symmetry appears with small perturbation and providing a density of states around S1. All their lowest excited states, corresponding to a local excitation from the donor and followed by charge-transfer transitions from donor to acceptor. Instead of a series of character transfer was observed through the three first excited states for both complexes, in the case of **5**-oligomer's structure the electron density is distributed over the whole molecule with higher densities on the fullerene core as shown in Figure 9.

The electronic Coulombic exchange (CE) contributions to the electronic transition energy terms describe the behavior of charge distributions during electronic excitations of molecular aggregates. The CE value expresses the stabilizing influence of electron-electron interactions on the excitation energy obtained after a configuration interaction calculation and can qualitatively estimate the bounding character of excitons.[65] In general, smaller CE values correspond to delocalized electron excitations with a collective character in the system, while higher values suggest localized electron transitions. Therefore, based on our approximation, it is possible to infer that the **5**-oligomer system generates less bounded excitons, thus favoring the separation of the electron-hole pair.

The energy conversion efficiency (η) in an organic solar cell is related to the amount of solar energy converted into electricity. One of the highest η values reported in the scientific literature corresponds to $PC_{61}BM$.[66] This magnitude depends on the LUMO energy of the material used as the electron acceptor in the electron transfer process. Therefore, if we compare the LUMO energy values calculated for **5**, as well as the similarity in the interactions with the thiophene oligomer related to $PC_{61}BM$,

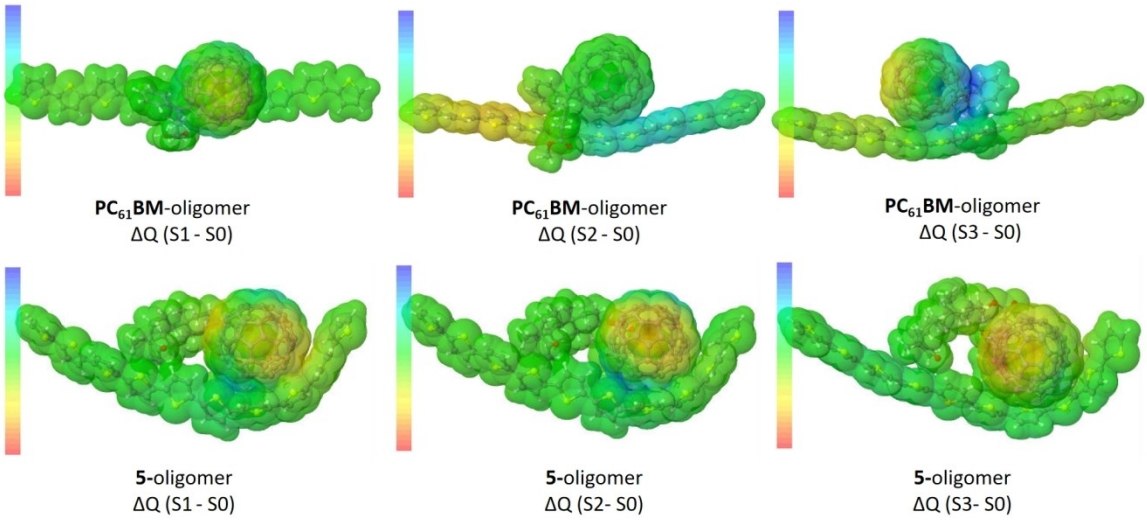

Figure 9. Calculated electronic charge maps for the excited states S1, S2 and S3 for the ground state S0 of the **5**-oligomer and $PC_{61}BM$-oligomer complexes at the CNDOL level.

together with its physical properties, the hybrid **5** can be considered a potential electron acceptor material with applications in materials science.

Conclusions

We have synthesized a novel fullerene-steroid hybrid derivative **5** using the Bingel–Hirsch methodology to compare its properties with $PC_{61}BM$, the reference structure as acceptor material in organic solar cells. An exhaustive spectroscopic and analytical study allowed the chemical structure of the new compound to be unambiguously determined. The electrochemical properties determined by cyclic voltammetry shown that the system exhibits three quasi-reversible reduction waves that are cathodically shifted compared to pristine C_{60}. TEM analysis evidences molecular aggregation and the formation of nanoparticles with a mean size of 8–13 nm. Thermogravimetric analysis indicated the thermal stability of the hybrid, required for organic photovoltaic devices. Additionally, DFT theoretical calculations predicted the most stable conformations of the synthesized steroid-fullerene derivative, showing that hydrogen bonds play a major role in the geometry of this hybrid molecule. The calculated dipole moments and quantum chemical parameters at DFT- PBE–D3 (BJ) / 6–311G (d,p) level evidences the good acceptor capability of the synthesized compound compared with $PC_{61}BM$. In addition, we applied the approximate CNDOL Fockian together with configuration interaction of single excitations (CIS), to investigate the electronic properties of the synthesized hybrid steroid-[60]fullerene and $PC_{61}BM$ with an oligomer of ten thiophene units as isolated supramolecular systems. Photoexcitation of the complex leads to an electron transfer in the system. Theoretical calculations, together with the experimental results obtained, demonstrated that hybrid **5** can be considered an appealing candidate for photovoltaic devices with applications in materials science.

Experimental Section

General: All reagents were commercial and used as supplied unless otherwise specified. Solvents were dried by standard procedures. All reactions were performed using an atmosphere of argon and oven-dried glassware. Reactions were monitored by thin-layer chromatography carried out on 0.25 mm silica gel plates (230–400 mesh). Flash column chromatography was performed using silica gel (60 Å, 32–63 μm). FTIR spectra were recorded in $CHCl_3$.^{1}H NMR spectra were recorded at 700 MHz, and ^{13}C NMR at 175 MHz; the one-bond heteronuclear correlation (HMQC) and the long-range ^{1}H–^{13}C correlation (HMBC) spectra were obtained by use of the inv4gs and the inv4gslplrnd programs. All MASS-ESI and HRMS-MALDI (dithranol as matrix) experiments were carried out in negative and positive detection modes. Microanalysis was performed with a 2400 CHN instrument. A high-performance liquid chromatography (HPLC) system (column dimensions: 4.6 mm×250 mm; flow rate 1.0 mL/min, injection volume 15 μL, eluent toluene/acetonitrile 9:1) was used to determine the purity of the compounds synthesized. The retention times (t_R) reported were determined at a wavelength of 320 nm. In Transmission electron microscopy (TEM), the aggregates were visualized using uranyl acetate negative staining. One drop of the clear solution was transferred to a TEM grid (copper grid, 3.0 mm, 200 mesh, coated with Formvar film), together with a drop of uranyl acetate (2% water solution) for 1 min, and allowed to dry. Analysis of stained grids was performed with a JEOL JEM 2100 (Tokyo, Japan). In the thermogravimetric analysis (TGA), the thermograms were registered in a TA Q500 (TA Instrument), with N_2 atmosphere through a gas purge system (with control of the mass flux). The sample was put on a platinum crucible and its analysis was carried out in an ultrasensitive thermobalance, in an oven of high temperature (20 to 1500 °C) using a temperature program of 1–40 °C/min (PlatinumTM Software). The electrochemical measurements were carried out on a three electrodes system. The measurements were realized in THF (0.1 M) at room temperature, employing a GCE as working electrode, Pt as counter electrode, $Ag/AgNO_3$ as reference electrode, $TBA{\cdot}PF_6$ (0.1 M) as supporting electrolyte, being the scan rate of 100 mV/s. Ferrocene was used as the inner reference, and all the potentials related to the pair Fc/Fc^+ were determined.

Theoretical Calculations: All computations were performed with the Gaussian 09 suite of programs,[67] and molecules were built with Avogadro.[68] The frontier orbitals HOMO/LUMO were visualized directly from the optimized structure with DFT/PBE[53] quantum mechanical calculation combined with D3(BJ) Grimme's dispersion correction,[55] with 6-311G(d,p) basis[55] set using Gaussview,[69] the graphical interface used with Gaussian. The optimized structure was confirmed to be minimum by harmonic vibrational frequency calculations performed at the same level of theory. Counterpoise method (CP)[70] was performed to correct the Basis Set Superposition Error (BSSE) in the calculation of energies of association for the complexes. The complexes' excited states energies and charge displacements were modeled by CNDOL approximation together with configuration interaction of single excitations (CIS).[36,63]

Synthesis of compounds

Synthesis of 3-oxy-(3β-5α-androstan-17-one)-3-oxopropanoic acid (2): To a stirred solution of 3β-hydroxi-5α-androstan-17-one, **1** (1.00 g, 2.66 mmol) in toluene (55 mL) was added Meldrum's acid (0.74 g, 5.14 mmol), heating it to reflux. The reaction mixture was monitored by TLC (*n*-hexane-ethyl acetate, 3:1). Once the reaction was finished (6 h) the solvent was evaporated in vacuum, using methanol to co-evaporate the toluene. The reaction crude was purified by flash chromatography using *n*-hexane/ethyl acetate (5:1) as the mobile phase. The product was obtained as a white solid, yield 0.64 g (1.70 mmol, 50%), mp 156–159 °C. ^{1}H NMR (700 MHz, $CDCl_3$, 25 °C): δ 4.80 (m, 1H, H3), 3.41 (s, 2H, $OCCH_2CO$), 2.44 (m, 1H, H16), 2.07 (m, 1H, H16), 1.93 (m, 1H, H15), 1.86 (m, 1H, H2), 1.80 (m, 1H, H12), 1.79 (m, 1H, H1), 1.75 (m, 1H, H7), 1.65 (m, 2H, H4, H11), 1.57 (m, 1H, H2), 1.55 (J = 11.5, 4.0 Hz, 1H, H8), 1.50 (m, 1H, H15), 1.42 (q, J = 12.4 Hz, 1H, H4), 1.34 (m, 1H, H7), 1.32 (d, J = 3.9 Hz, 1H, H6), 1.31 (m, 1H, H14), 1.30 (m, 1H, H11), 1.29 (m, 1H, H6), 1.27 (m, 1H, H12), 1.20 (m, 1H, H5), 1.05 (m, 1H, H1), 0.85 (s, 6H, H18, H19), 0.72 (td, J = 12.2, 4.0 Hz, 1H, H9) ppm. ^{13}C NMR{1H} (175 MHz, $CDCl_3$, 25 °C): δ 221.60 (C17), 169.70 (C=O), 167.58 (C=O), 75.86 (C3), 54.37 (C9), 51.46 (C14), 47.94 (C13), 44.73 (C5), 40.33 ($OCCH_2CO$), 36.72 (C1), 35.99 (C16), 35.75 (C10), 35.13 (C8), 33.76 (C4), 31.62 (C12), 30.91 (C7), 28.35 (C6), 27.30 (C2), 21.91 (C15), 20.60 (C11), 13.96 (C18), 12.35 (C19) ppm. IR ($CHCl_3$): ν 3150; 2935; 2855; 1734, (C=O); 1472; 1451; 1375; 1061;

735 cm^{-1}. MS-ESI: $[M+Na]^+$ *m/z* for $C_{22}H_{32}O_5$ 399.1. Anal. Calcd for $C_{22}H_{32}O_5$: C, 70.18; H, 8.57. Found: C, 70.22; H, 8.61.

3β-benzylmalonate-5α-androstan-17-one (4): In a flask of 50 mL were dissolved 0.2 g (0.53 mmol) of compound **2** in 10 mL of dry chloroform. Afterward 80 μL (1.10 mmol) of thionyl chloride ($SOCl_2$) was added, and the reaction mixture was heated to reflux during 8 h. The reaction was monitored employing *n*-hexane/ethyl acetate (1:1) as mobile phase by TLC. Lapsed the aforementioned time, the reaction was stopped and the solvent evaporated under reduced pressure to obtain a viscous brown liquid (**3**). At the same time in a flask of 50 mL, 60 μL (0.58 mmol) of benzyl alcohol were dissolved in 20 mL of dry dichloromethane. To the resulting solution 0.06 g (0.49 mmol) of DMAP were added, and the reaction was cooled in an ice bath to 0 °C. Subsequently compound **3** was added and the reaction mixture was then stirred for 2 h at room temperature under an argon atmosphere. After this period of time, the ice bath was withdrawn and the agitation was kept overnight. Once the reaction concluded, was washed with water. The organic phase was dried with anhydrous Na_2SO_4, and evaporated to vacuum. The reaction mixture was purified by column chromatography on silica gel, employing *n*-hexane/ethyl acetate (5:1) as mobile phase. Yield: 0.1 g (0.21 mmol), 42%. Viscous yellow liquid.^{1}H NMR (700 MHz, $CDCl_3$, 25 °C): δ 7.36 (m, 2H, H3′, H5′), 7.34 (m, 2H, H2′, H6′), 7.30 (m, 1H, H4′), 5.18 (s, 2H, CH_2O), 4.73 (m, 1H, H3), 3.39 (s, 2H, $OCCH_2CO$), 2.43 (dd, *J* = 19.3, 8.9 Hz, 1H), 2.06 (dt, *J* = 18.9, 9.1 Hz, 1H, H16), 2.06 (dt, *J* = 18.9, 9.1 Hz, 1H, H16), 1.92 (m, 1H, H15), 1.80 (m, 1H, H2), 1.78 (m, 1H, H1), 1.71 (m, 1H, H7), 1.65 (m, 1H, H11), 1.64 (m, 1H, H4), 1.56 (m, 1H, H8), 1.52 (m, 1H, H15), 1.49 (m, 1H, H2), 1.35 (m, 1H, H4), 1.33 (m, 1H, H7), 1.31 (m, 1H, H6), 1.30 (m, 1H, H14), 1.28 (m, 1H, H6), 1.25 (m, 1H, H11), 1.21 (m, 2H, H12), 1.17 (m, 1H, H5), 1.02 (m, 1H, H1) 0.96 (m, 1H, H7), 0.85 (s, 3H, H19), 0.82 (s, 3H, H18), 0.70 (m, 1H, H9) ppm. ^{13}C NMR{1H} (175 MHz, $CDCl_3$, 25 °C): δ 221.20 (C17), 166.51 (C═O), 165.92 (C═O), 135.28 (C1′), 128.54 (C3′), 128.40 (C4′), 128,35 (C2′), 74.88 (C3), 67.12 (CH_2O), 54.23 (C9), 51.32 (C14), 47.75 (C13), 44.56 (C5), 41.96 ($OCCH_2CO$), 36.59 (C1), 35.82 (C16), 35.59 (C10), 34.99 (C8), 33.61 (C4), 31.48 (C12), 30.76 (C7), 28.19 (C6), 27.14 (C2), 21.75 (C15), 20.44 (C11), 13.79 (C18), 12.19 (C19) ppm. IR ($CHCl_3$): ν 2923; 2854; 1729, (C═O); 1498, 1453; 1376; 1182; 1060; 737 cm^{-1}. MS-ESI: $[M+Na]^+$ *m/z* for $C_{29}H_{38}O_5$ 489.2. Anal. Calcd for $C_{29}H_{38}O_5$: C, 74.65; H, 8.21. Found: C, 74.69; H, 8.26.

61-(benzyloxycarbonyl)-61-(3β-O-carbethoxy-5α-androstan-17-one)methano[60]fullerene (5): A solution of C_{60} (49 mg, 0.68 mmol) in dry toluene (50 mL) was prepared. Subsequently, 3β-benzylmalonate-5α-androstan-17-one (**4**) (46 mg, 0.99 mmol), CBr_4 (30 mg, 0.90 mmol), and diazabicyclo[4.2.0]undec-7-ene (DBU, 0.17 mL, 1.14 mmol) were added in that order. The reaction mixture was stirred for 2 h at room temperature under an argon atmosphere. Subsequently, water was added, and the residue was extracted with toluene. The combined extracts were dried with $MgSO_4$ and filtered, and the solvent was removed under reduced pressure. Purification of the product was achieved by column chromatography on silica gel, first with CS_2 to elute unreacted C_{60} and dichloromethane to elute the corresponding functionalized fullerene **5**, yield of isolate pure product 54 mg (0.46 mmol, 66%), amorphous brown solid. HPLC: toluene/acetonitrile (9:1), flow rate 1 mL/min, t_R = 5.71 min. 1H NMR (700 MHz, $CDCl_3$, 25 °C): δ 7.53 (d, *J* = 7.1 Hz, 2H, H3′, H5′), 7.41 (m, 3H, H2′, H6′, H4′), 5.52 (m, 2H, CH_2O), 5.08 (m, 1H, H3), 2.44 (m, 1H, H16), 2.08 (m, 2H, H2, H16), 1.95 (m, 1H, H15), 1.91 (m, 1H, H4), 1.89 (m, 1H, H1), 1.83 (m, 1H, H12) 1.82 (m, 1H, H7), 1.78 (m, 1H, H2), 1.70 (m, 1H, H11), 1.68 (m, 1H, H4), 1.57 (m, 1H, H8), 1.51 (m, 1H, H15), 1.43 (m, 1H, H6), 1.42 (m,1H, H6), 1.40 (m, 1H, H11), 1.35 (m, 1H, H5), 1.31 (m, 1H, H14), 1.25 (m, 1H, H1), 1.05 (m, 1H, H7), 0.88 (s, 3H, H18), 0.86 (s, 3H, H19), 0.71 (m, 1H, H9) ppm. ^{13}C NMR {^{1}H} (175 MHz, $CDCl_3$, 25 °C): δ 221.19 (C17), 163.51 (C═O), 162.92 (C═O), [145.23, 145.15, 144.85, 144.66, 144.60, 144.58, 144.54, 143.85, 142.99, 142.94, 142.18, 141.89, 141.84, 140.90, 139.06, 139.00] C_{60}, 134.60 (C1′), 129.28 (C3′), 128.98(C2′), 128.70 (C4′), 77.23 (C3), 71.60 (Csp^3-C_{60}), 71.58 (Csp^3-C_{60}), 68.87 (CH_2O), 54.20 (C9), 52.15 (C61), 51.31 (C14), 47.77 (C13), 44.70 (C5), 36.64 (C1), 35.85 (C16), 35.68 (C10), 35.01 (C8), 33.53 (C4), 31.49 (C12), 30.78 (C7), 28.24 (C6), 27.15 (C2), 21.78 (C15), 20.49 (C11), 13.82 (C18), 12.35 (C19) ppm. IR ($CHCl_3$): ν 2923; 2854; 1737, (C═O); 1459; 1181; 1057; 729 cm^{-1}. HRMS (MALDI-TOF): *m/z:* $[M-H]^{\bullet-}$ calcd for $C_{89}H_{35}O_5$ 1184.25625, found, 1184.25532.

Acknowledgements

Financial support by the Spanish Ministry of Science and Innovation (MICIN) through projects PID2020-114653RB-I00 and PID2020-115120GB-I00 /AEI /10.13039/ 501100011033, PNCB of MES, Cuba (PN223LH010-019), and Yachay Tech Internal Project (CHEM20-08). Y. Perez-Badell acknowledges the Department of Applied Physical Chemistry of the Universidad Autónoma de Madrid for providing the computational resources used for calculations.

Conflict of Interests

The authors declare no conflict of interest.

Data Availability Statement

The data that support the findings of this study are available in the supplementary material of this article.

Keywords: cyclic voltammetry · density functional calculations · electron transport · fullerenes · steroids

[1] S. J. Davis, K. Caldeira, H. D. Matthews, *Science* **2010**, *329*, 1330–1333.
[2] M. Höök, X. Tang, *Energy Policy* **2013**, *52*, 797–809.
[3] T. A. Faunce, W. Lubitz, A. W. Rutherford, D. MacFarlane, G. F. Moore, P. Yang, D. G. Nocera, T. A. Moore, D. H. Gregory, S. Fukuzumi, K. B. Yoon, F. A. Armstrong, M. R. Wasielewski, S. Styring, *Energy Environ. Sci.* **2013**, *6*, 695–698.
[4] B. K. Ghosh, C. N. J. Weoi, A. Islam, S. K. Ghosh, *Energy Rev.* **2018**, *82*, 1990–2004.

[5] M. K. Assadi, S. Bakhoda, R. Saidur, H. Hanaei, *Renewable Sustainable Energy Rev.* **2017**, *81*, 2812–2822.
[6] K. Yoshikawa, H. Kawasaki, W. Yoshida, T. Irie, K. Konoshi, K. Nakano, T. Uto, D. Adachi, M. Kanematsu, H. Uzu, K. Yamamoto, *Nat. Energy* **2017**, *2*, 17032.
[7] M. Ghorab, A. Fattah, M. Joodaki, *Optik* **2022**, *267*, 169730.
[8] S. B. Darling, F. You, *RSC Adv.* **2013**, *3*, 17633–17648.
[9] F. C. Krebs, N. Espinosa, M. Hosel, R. R. Sondergaard, M. Jorgensen, *Adv. Mater.* **2014**, *26*, 29–38.
[10] K. Zhang, Z. Hu, C. Sun, Z. Wu, F. Huang, Y. Cao, *Chem. Mater.* **2017**, *29*, 141–148.
[11] L. T. Dou, Y. S. Liu, Z. R. Hong, G. Li, Y. Yang, *Chem. Rev.* **2015**, *115*, 12633–12665.
[12] A. G. Aberle, *Prog. Photovoltaics* **2000**, *8*, 473–487.
[13] G. Lan, Y. Fan, W. Shi, E. You, S. S. Veroneau, W. Lin, *Nat. Catal.* **2022**, *5*, 1–13.
[14] A. J. Heeger, *Adv. Mater.* **2014**, *26*, 10–28.
[15] N. Li, D. Baran, G. D. Spyropoulos, H. Zhang, S. Berny, M. Turbiez, T. Ameri, F. C. Krebs, C. J. Brabec, *Adv. Energy Mater.* **2014**, *4*, 1400084.
[16] S. Rafique, S. M. Abdllah, K. Sulaiman M Iwamoto, *Renewable Sustainable Energy Rev.* **2018**, *84*, 43–53.
[17] H. Derouiche, V. Djara, *Sol. Energy Mater. Sol. Cells* **2007**, *91*, 1163–1167.
[18] D. P. Hagberg, T. Marinado, K. M. Karlsson, K. Nonomura, *J. Org. Chem.* **2007**, *72*, 9550–9556.
[19] Z. Xiao, X. Jia, L. Ding, *Sci. Bull.* **2017**, *62*, 1562–1564.
[20] L. X. Chen, *ACS Energy Lett.* **2019**, *4*, 2537–2539.
[21] C. W. Tang, *Appl. Phys. Lett.* **1986**, *48*, 183–185.
[22] A. V. Mumyatov, P. A. Troshin, *Energies* **2023**, *16*, 1924.
[23] G. Garcia-Belmonte, P. P. Boix, J. Bisquert, M. Lenes, H. J. Bolink, A. La Rosa, S. Filippone, N. Martín, *J. Phys. Chem. Lett.* **2010**, *1*, 2566–2571.
[24] J. C. Hummelen, B. W. Knight, F. LePeq, F. Wudl, J. Yao, Ch. L. Wilkins, *J. Org. Chem.* **1995**, *60*, 532538.
[25] P. R. Berger, M. Kim, *Renewable Sustainable Energy Rev.* **2018**, *10*, 013508.
[26] P. A. Troshin, H. Hoppe, J. Renz, M. Egginger, J. Y. Mayorova, A. E. Goryachev, A. S. Peregudov, R. N. Lyubovskaya, G. Gobsch, N. S. Sariciftci, V. Razumov, *Adv. Funct. Mater.* **2009**, *19*, 779–788.
[27] C. Tian, E. Castro, G. Betancourt-Solis, Z. Nan, O. Fernandez-Delgado, S. Jankuru, L. Echegoyen, *New J. Chem.* **2018**, *42*, 2896–2902.
[28] E. Castro, J. Murillo, O. Fernandez-Delgado, L. Echegoyen, *J. Mater. Chem. C.* **2018**, *6*, 2635–2651.
[29] O. Fernandez-Delgado, P. S. Chandrasekhar, N. Cano-Sampaio, Z. C. Simon, A. R. Puente-Santiago, F. Liu, L. Echegoyen, *J. Mater. Chem. C.* **2021**, *9*, 10759–10767.
[30] M. Suarez, K. Makowski, R. Lemos, L. Almagro, M. Á. Herranz, D. Molero, H. Rodriguez, N. Martín F Albericio, Y. Murata, N. Martín, *ChemPlusChem.* **2021**, *86*, 972–981.
[31] D. Alonso, D. Hernandez-Castillo, L. Almagro, R. Gonzalez-Aleman, D. Molero, M. A. Herranz, E. Medina-Paez, J. Coro, R. Martinez-Alvarez, M. Suarez, N. Martín, *J. Org. Chem.* **2020**, *85*, 2426–2437.
[32] P. Nitschke, B. Jarząbek, M.-D. Damaceanu, A.-E. Bejan, P. Chaber, *Spectrochim. Acta A Mol. Biomol. Spectrosc.* **2021**, *248*, 119242.
[33] K. Sen, R. Crespo-Otero, O. Weingart, W. Thiel, M. Barbatti, *J. Chem. Theory Comput.* **2013**, *9*, 533–542.
[34] P. Schilinsky, C. Waldauf, C. J. Brabec, *Adv. Funct. Mater.* **2006**, *16*, 1669–1672.
[35] S. Krishnan, K. Senthilkumar, *Phys. Chem. Chem. Phys.* **2021**, *23*, 27468–27476.
[36] Y. Pérez-Badell, L. Montero-Cabrera, *Mol. Phys.* **2023**, *121*, e2151945.
[37] T. Duan, Q. Chen, D. Hu, J. Lu, D. Yu, G. Li, S. Lu, *Trends Chem.* **2022**, *4*, 773–791.
[38] F. Diederich, L. Isaacs, *J. Chem. Soc.-Perkin Trans.* **1994**, 391–394.
[39] N. M. Thong, T. C. Ngo, D. Q. Dao, T. Duang, Q. T. Tran, P. C. Nam, *J. Mol. Model.* **2016**, *22*, 113.
[40] C. Du, J. Xu, Y. Li, W. Xu, D. Zhu, *Chin. Sci. Bull.* **2001**, *46*, 1156–1159.
[41] A. Bianco, M. Maggini, G. Scorrano, C. Toniolo, G. Marconi, C. Villani, M. Prato, *J. Am. Chem. Soc.* **1996**, *118*, 4072–4080.
[42] B. W. Larson, J. B. Whitaker, X.-B. Wang, A. A. Popov, G. Rumbles, N. Kopidakis, S. H. Strauss, O. V. Boltalina, *J. Phys. Chem. C* **2013**, *117*, 14958–14964.
[43] C. M. Cardona, W. Li, A. E. Kaifer, D. Stockdale, G. C. Bazan, *Adv. Mater.* **2011**, *23*, 2367–2371.
[44] M. Á. Herranz, F. Diederich, L. Echegoyen, *Eur. J. Org. Chem.* **2004**, 2299–2316.
[45] D. M. Guldi, M. Maggini, E. Menna, G. Scorrano, P. Ceroni, M. Marcaccio, F. Paolucci, S. A. Roffia, *Chem. Eur. J.* **2001**, *7*, 1597–1605.
[46] S. A. Lerke, B. A. Parkinson, D. H. Evans, P. J. Fagan, *J. Am. Chem. Soc.* **1992**, *114*, 7807–7813.
[47] Z. Liang, X. Cheng, Y. Jiang, J. Yu, X. Xu, Z. Peng, L. Bu, Y. Zhang, Z. Tang, M. Li, L. Ye, Y. Geng, *ACS Appl. Mater. Interfaces* **2021**, *13*, 61487–61495.
[48] Y. Li, *Acc. Chem. Res.* **2012**, *5*, 723–733.
[49] A. Ruiz, M. Suárez, N. Martin, F. Albericio, H. Rodríguez, *Beilstein J. Nanotechnol.* **2014**, *5*, 374–379.
[50] R. Lemos, F. Ortiz, L. Almagro, K. Makowski, N. Martin, F. Albericio, M. Suárez, H. Rodríguez, *Surf. Interface Anal.* **2022**, *54*, 1041–1051.
[51] F. C. Jamieson, E. Buchaca-Domingo, T. McCarthy-Ward, M. Heeney, N. Stingelich, J. R. Durrant, *Chem. Sci.* **2012**, *3*, 485–492.
[52] M. Tessaroloa, A. Guerrero, D. Gedefaw, M. Bolognesi, M. Prosaa, X. Xu, M. Mansour, E. Wang, M. Seri, M. R. Anderssonc, M. Muccini, G. Garcia-Belmonte, *Sol. Energy Mater. Sol. Cells* **2015**, *141*, 240–247.
[53] J. P. Perdew, K. Burke, M. Ernzerhof, *Phys. Rev. Lett.* **1996**, *77*, 3865–3868.
[54] S. Grimme, S. Ehrlich, L. Goerigk, *J. Comput. Chem.* **2011**, *32*, 1456–1465.
[55] R. Ditchfield, W. J. Hehre, J. A. Pople, *J. Chem. Phys.* **1971**, *54*, 724–728.
[56] L. Almagro, R. Lemos, K. Makowski, H. Rodríguez, O. Ortiz, W. Cáceres, M. Á. Herranz, D. Molero, R. Martínez-Álvarez, M. Suárez, N. Martín, *Eur. J. Org. Chem.* **2020**, 5926–5937.
[57] L. Almagro, D. Hernández-Castillo, O. Ortiz, D. Alonso, A. Ruiz, J. Coro, M. Á. Herranz, D. Molero, R. Martínez-Álvarez, M. Suárez, N. Martín, *Eur. J. Org. Chem.* **2018**, 4512–4522.
[58] E. M. Pérez, N. Martín, *Chem. Soc. Rev.* **2015**, *44*, 6425–6433.
[59] C. Tian, C. Sun, J. Chen, P. Song, E. Hou, P. Xu, Y. Liang, P. Yang, J. Luo, L. Xie, Z. Wei, *Nanomaterials* **2022**, *12*, 532.
[60] H. Wang, Y. He, Y. Li, H. Su, *J. Phys. Chem. A.* **2012**, *116*, 255–262.
[61] M. Hagar, H. A. Ahmed, G. Aljohani, O. A. Alhaddad, *Int. J. Mol. Sci.* **2020**, *21*, 3922.
[62] M. C. Sharber, D. Mühlbacher, M. Koppe, P. Denk, C. Waldauf, A. J. Heeger, C. J. Brabec, *Adv. Mater.* **2006**, *17*, 789–794.
[63] J. C. Dobrowolski, M. E. Jamróz, *RSC Adv.* **2018**, *8*, 2116.
[64] L. A. Montero-Cabrera, U. Röhrig, J. A. Padron-García, R. Crespo-Otero, A. L. Montero-Alejo, J. M. García de la Vega, M. Chergui, U. Röthlisberger, *J. Chem. Phys.* **2007**, *127*, 145102.
[65] A. L. Montero-Alejo, M. E. Fuentes, L. A. Montero, J. M. G. de la Vega, *Chem. Phys. Lett.* **2011**, *502*, 271–276.
[66] Y. Zhang, T. P. Basel, B. R. Gautam, X. Yang, D. J. Mascaro, F. Liu, Z. V. Vardeny, *Nat. Commun.* **2012**, *3*, 1043.
[67] M. J. Frisch, G. W. T., H. B. Schlegel, G. E. Scuseria, M. A. Robb, J. R. Cheeseman, G. Scalmani, V. Barone, B. Mennucci, G. A. Petersson, H. Nakatsuji, M. Caricato, X. Li, H. P. Hratchian, A. F. Izmaylov, J. Bloino, G. Zheng, J. L. Sonnenberg, M. Hada, M. Ehara, K. Toyota, R. Fukuda, J. Hasegawa, M. Ishida, T. Nakajima, Y. Honda, O. Kitao, H. Nakai, T. Vreven, J. A. Montgomery Jr., J. E. Peralta, F. Ogliaro, M. Bearpark, J. J. Heyd, E. Brothers, K. N. Kudin, V. N. Staroverov, R. Kobayashi, J. Normand, K. Raghavachari, A. Rendell, J. C. Burant, S. S. Iyengar, J. Tomasi, M. Cossi, N. Rega, J. M. Millam, M. Klene, J. E. Knox, J. B. Cross, V. Bakken, C. Adamo, J. Jaramillo, R. Gomperts, R. E. Stratmann, O. Yazyev, A. J. Austin, R. Cammi, C. Pomelli, J. W. Ochterski, R. L. Martin, K. Morokuma, V. G. Zakrzewski, G. A. Voth, P. Salvador, J. J. Dannenberg, S. Dapprich, A. D. Daniels, Ö. Farkas, J. B. Foresman, J. V. Ortiz, J. Cioslowski, D. J. Fox, Gaussian 09, Revision E.01, Gaussian, Inc., Wallingford CT, **2013**.
[68] M. D. Hanwell, D. E. C., D. C. Lonie, T. Vandermeersch, E. Zurek, G. R. Hutchison, Avogadro: an advanced semantic chemical editor, visualization, and analysis platform, *J. Cheminf.* **2012**, *4*, 17.
[69] R. D. Dennimgton II, T. A. Keith, J. M. Milam, *GaussView 6.0.16*, Semichem, Inc. 2000–2016.
[70] S. F. Boys, F. Bernardi, *Mol. Phys.* **1970**, *19*, 553–556.

Manuscript received: August 20, 2023
Revised manuscript received: October 30, 2023
Accepted manuscript online: November 6, 2023
Version of record online: December 14, 2023